鞍山市第三届学术年会论文集

李　平　主编

辽宁科学技术出版社
沈 阳

需要全本请访问 www.ertongbook.com

主　编：李　平
副主编：王尔莉　程　斌　杨　建　刘　军　刘东风
　　王　宁
编　委：（以姓氏笔画为序）
　　成之光　任瑞平　李心禄　连　琦　肖爱民
　　宋　华　张素艳　赵素华　俞美蓉　宫元春
　　唐　洁　曹　林　章　杨　黄　强　惠忠波

© 2011　版权归鞍山市科学技术协会所有，授权辽宁科学技术出版社使用

图书在版编目（CIP）数据

鞍山市第三届学术年会论文集 / 李平主编. —沈阳：辽宁科学技术出版社，　011.1
ISBN 978-7-5381-7267-6

Ⅰ. ①鞍… Ⅱ. ①李… Ⅲ. ①科学技术—学术会议—文集
Ⅳ. ①N53

中国版本图书馆CIP数据核字（2010）第249006号

出版发行：辽宁科学技术出版社
　　（地址：沈阳市和平区十一纬路29号　邮编：110003）
印 刷 者：沈阳新华印刷厂
幅面尺寸：185mm × 260mm
印　　张：18
字　　数：400千字
印　　数：1 ~ 1000
出版时间：2011年1月第1版
印刷时间：2011年1月第1次印刷
责任编辑：李伟民　修吉航
封面设计：嵘　嵘
责任校对：王玉宝

书　　号：ISBN 978-7-5381-7267-6
定　　价：90.00元

前　言

当今世界，科技已成为支撑和引领经济发展和社会进步的重要因素。科技发展从来没有像今天这样深刻地影响着社会生产和生活的方方面面，从来没有像今天这样深刻地影响着人们的思想观念和生活方式，从来没有像今天这样深刻地影响着国家和民族的前途命运。

本届学术年会坚持以科学发展观为指导，秉承普及科学知识、弘扬科学精神、传播科学思想和科学方法的宗旨，紧紧围绕“低碳经济与可持续发展”的主题，针对科技、经济和社会发展各领域中的综合性、交叉性、前沿性学术问题进行交流和研讨，促进不同学科、行业的交流；展示全市广大科技工作者的最新科研成果，展望科技发展前景，为实现我市经济社会又好又快发展提供智力支撑和保证。

本届学术年会共征集论文162篇，经有关专家评审，评选出83篇论文出版。其中，特等奖4篇、一等奖9篇、二等奖30篇、三等奖40篇。内容涉及工程技术、环境、资源、材料、医学、生物技术及农、林、牧等多学科和领域。评委对本届年会论文给予了高度评价。

本届年会的论文征集工作得到了各学会、大专院校、科研院所的大力支持，论文评委会的专家在论文评审过程中能做到平等公正、坚持标准、严格评定，保证了优秀论文的水平。借此机会，对他们付出的辛勤劳动表示由衷的感谢。

本论文集的编辑出版尚有不尽如人意之处，诚望论文作者和广大读者予以谅解。

编　者

2010年10月

目 录

Compressive residual stress induced by water cavitation peening: A finite element analysis …… B. Han D.Y. Ju 001
我国农民体育健身工程的建设现状与发展策略研究 …… 刘志敏 丁振峰 程丽华 014
Preparation of homodispersed nano zirconia …… Shaoyan Wang Xiaoan Li Yuchun Zhai Kaiming Wang 021
Direct palladium-catalyzed C-3 arylation of indoles …… Zhiqiang Zhang Zhizhi Hu Zhixiao Yu Peng Lei Haijun Chi Yue Wang Ren He …… 032
不同工艺路线超低碳钢洁净度分析 …… 常桂华 栗 红 陈本文 赵 刚 王向辉 040
Study on the Polishing Characteristics of the Magnetic Abrasives Finishing to the Slender Pipe …… Y. Chen F. Yan C. Q. Zhu 045
电感耦合等离子体原子发射光谱法测定高炉渣中硼 … 顾继红 于媛君 王赫男 杨丽荣 050
HTP工艺条件下700 N/mm²级别中厚板组织与性能 …… 侯华兴 杨 颖 张 涛 刘 明 055
添加熔剂对球团矿还原膨胀性能的影响 …… 李艳茹 李金莲 张立国 任 伟 062
RH-TB精炼脱碳过程数学模型 …… 赵成林 王丽娟 黄玉平 李广帮 张维维 067
磁、赤铁矿混合烧结技术研究 …… 周明顺 尚 策 翟立委 任 伟 刘 杰 073
The Improved Algorithm of ART2 in Data Mining …… Li Liangjun Zhang Bin Che Yuanyuan 078
饮用水的二次污染及其对策 …… 艾 欣 陈 瑾 084
南果梨红果皮中花青素提取工艺研究 …… 陈 华 辛 广 张 博 杨佳颖 086
构建生态型绒山羊生产模式的思考与实践……丁家刚 丁 巍 091
激励理论及其在酒店员工管理中的应用 …… 谷 珺 094

气基竖炉直接还原技术的发展 …… 胡俊鸽 097
含Mo微合金化钢控轧控冷工艺模拟试验研究 … 李桂艳　赵宝纯　庞兆夫　马慧霞 102
超声波技术在白灵菇多糖提取工艺中的应用 …… 李书倩　辛　广　刘长江 107
分析美国体育产业的发展谈我国体育市场 …… 李迎春 113
眼眶爆裂性骨折手术并发症的分析与治疗 …… 林　雪　张明欣　敖海生 116
美国次贷危机解析 …… 林　煜 119
The effects of a single stage-structured population model with impulsive toxin input and time delays in a polluted environment ……Bing Liu Lei Zhang Qian Zhang 122
CC2000A地调自动化系统在鞍山供电公司的应用 ……鹿　军　张　博　曹　佳 136
超声波治疗急性脑梗死临床疗效观察及对血浆NO、ET变化的影响
…… 王复新　彭守仙　张淑萍　侯丽淳　关雪莲　刘玉荣　龚光清 142
Experimental Study on 830MPa-grade Pipeline Steel Containing Chromium
…… Ren Yi Zhang Shuai Wang Shuang Liu Wenyue 146
Nb-V-Ti微合金钢细晶和粗晶奥氏体晶粒长大的比较
…… 沙庆云　乔立峰　许荣杰　黄国建　孙祖庆 155
凹底平板热钢保温车研制使用 …… 宋正学 163
基于粒子群优化算法的球磨机制粉系统PID-ANN 解耦控制器
…… 王介生　丛峰武　张　勇 170
外国技术创新发展历史比较及启示……吴芷静 177
IPF的HRCT表现与肺功能及支气管肺泡灌洗液细胞学相关性研究
…… 肖振平　黎　庶　李振华　李今朝 183
64排螺旋CT冠状动脉造影临床应用价值 …… 徐娅莎　吕杰文　陈月洁　庞　钢 190
高油大豆“岫豆94–11”高产栽培技术 …… 徐永兴　孙凤荣 202
户用玻璃钢自动出料沼气池技术研究及应用 …… 杨海玉 205
巴西VALE低硅铁矿粉烧结性能研究… 翟立委　周明顺　任　伟　刘　杰　袁　慧 208
IF钢冷轧板表面条状缺陷 …… 张维维　李晓伟　吕春风 213
catena-Poly［［［aquasilver（I）］-μ-4, 4′-bipyridine-k^2N, N'］4-aminobenzoate nitrate hydrate］ …… Yong-Mei Zhang Dong-Yan Hou Guang Xin Tie-Chun Li 218
A refined theory of torsional deformation of a circular shaft
…… Baosheng Zhao　Yang Gao　Xiue Wu 228
亚低温对成年大鼠fCIRI后内源性神经干细胞的影响
…… 赵桂梅　吴家幂　张希庆　郭宇林　文　华　张　轩　储照虎 239

需要全本请访问 www.ertongbook.com

fCIRI对成年大鼠内源性神经干细胞的影响…… 赵桂梅 吴家幂 244
饲料质量对畜产品品质的影响 …… 韩立辉 249
双酚芴合成的工艺研究 …… 尚纯颖 253
设计专业构成课程的语义转化教学探索 …… 梅 云 256
载脂蛋白M基因单体型与脑梗死关系的研究 …… 韩秀杰 贾建平 259
再生医学——自体骨髓造血干细胞移植在临床多领域的应用
…… 邵巧兵 张 昆 李玉芳 曹 辉 259
自体外周血干细胞动脉腔内联合缺血部位肌肉移植治疗糖尿病足研究
…… 于华峰 张家齐 赵 荣 马云辉 260
CyclinE在骨肉瘤、骨巨细胞瘤和骨软骨瘤中的表达研究
…… 朱海心 刘 刚 李广辉 于海斌 260
66 kV小坨数字化变电站设计与实现 …… 刘 君 261
紫草人工栽培技术研究 …… 栾洪涛 郝春波 张 艳 261
制冷压缩机行业用冷轧电工钢产品的生产技术…高振宇 罗 理 张智义 李亚东 262
硫酸锌对镀锌钢板中铬酸盐转化膜检测的影响…陈义庆 徐承明 徐小连 肖 宇 262
基于OCCI和MapX的GIS应用系统的开发 …… 李光师 263
慢性乙型肝炎患者IFN治疗与HBV DNA前C区变异关系的研究
…… 孙国君 张艳红 宋春玲 于福军 贺志华 刘德刚 263
肝门部胆管癌手术入路方式选择的临床研究 …… 刘吉盛 264
鞍山市功能性消化不良患者症状与精神心理及生活质量的流行病学调查研究
…… 卢艳萍 邵巧兵 264
c-erbB-2、bcl-2、bax和p53在大肠癌中的表达及其临床意义 …… 马文亮 富艳辉 265
环锯法后路椎间植骨融合治疗成人Ⅰ°、Ⅱ°腰椎滑脱的临床研究 …… 陈林林 266
雾化吸入粒细胞–巨噬细胞集落刺激因子治疗肺转移癌的临床试验研究
…… 吴登斌 王文萍 高晶晶 王忠帅 艾春玲 高广营 266
奥扎格雷钠与阿司匹林联用治疗急性脑梗死临床研究 …… 徐 萍 267
瑞芬太尼复合咪唑安定用于烧伤换药麻醉的临床观察 …… 张恒文 268
66 kV SVC装置在220 kV东鞍山变电站的应用研究 … 杨 松 张 旭 刘俊德 268
数字化网络变电站现场技术简析 …… 刘欣海 269
浅谈子猪黄白痢的发病原因及综合防治 …… 侯彦波 269
发酵蛋白饲料的研制 …… 郭洪伟 269
浅析“布病”发生的原因及防控对策 …… 卜仁英 270

利用生物技术常规选育抗螟玉米自交系杂交种的研究初报 …… 佟　旭 270
基于有限元和位错错密度相结合的模型求解空化水喷丸处理后残余应力分布 …韩　冰 271
鞍钢自产铁精矿原料特性对球团成球性能的影响 …… 周　伟　田嘉印 271
鞍钢冷轧无取向电工钢生产技术探讨 …… 高振宇　罗　理　张智义　李文权 272
鞍钢烘烤硬化高强深冲冷轧汽车板的研究进展……刘军友 272
ASP小交叉轧制工艺研究 …… 史乃安　邹　波　吴胜田 273
添加熔剂对球团矿还原膨胀率的影响 …… 李艳茹 273
浅谈人口疏散基地建设 …… 胡殿林 274
数字人防城市动态监视系统的虚拟化构建 …… 粟　话 274
多元反馈教学法在高校体育专业教学中对学生能力的培养 …… 张　岚 274
倾斜海底露头覆盖层对滨海承压海水层系统水头波动影响的数字模拟 …… 刘　双 275
种子季节性传播 …… 张玉娟 275
小麦酯酶的纯化研究 …… 翁　霞 276
冷香玫瑰在鞍山地区的栽培试验 …… 胡力男　王春静 276
科普展品“奇妙的光阀” …… 蒋全喜 277
中医穴位疗法综合治疗现代疾病的临床研究 …… 冯　莉 277
藤仙甲治疗类风湿性关节炎100例临床研究
…… 姜玉娟　葆　艳　潘丽坤　张　镇　王志伏 277
胸腺肽α_1对维持性血液透析患者发生感染的预防作用 …… 刘运明 278

Compressive residual stress induced by water cavitation peening: A finite element analysis

B. Han D.Y. Ju

abstract: Water cavitation peening is a recent promising method in surface treatment. It has the potential to induce compressive residual stresses that benefit the fatigue life of components similar to the other peening process. In this paper, a novel method, proposed for predicting residual stress induced on the materials subsurface treated with water cavitation peening, is presented. A bilinear elastic-plastic finite element analysis was conducted to predict to residual stresses. The three-dimensional model was based on the classical bilinear kinematic hardening model that uses two slopes (elastic and plastic) to represent the stress-strain behavior of a material. The approach provided prediction of magnitude and depth of residual stress fields in pure titanium. Effect of applied impact pressures on the residual stresses was also presented. Results of the finite element analysis modeling were in good agreement with that of the experimental measurements.

Keywords: Water cavitation peening; Finite element analysis; Residual stress; X-ray diffraction

1 Introduction

Water cavitation peening (WCP) is a surface treatment process that can impart compressive residual stresses in the surface and subsurface layers for enhancing the fatigue life of components. In this field, similar method also is referred to as water jet peening (WJP). In those processes, high-velocity water with abundant air bubbles continuously impinges over the surface. These bubbles' blasts produce high peak loads that can cause localized plastic deformation of material and stretching of the layers of the surface. Upon unloading, the elastically stressed sub surface layers tend to recover to original state. But the continuity of material in both elastic and plastic zones does not permit this to happen. Consequently, a compressive residual stress followed by tensile stress is trapped in the treated component. Therefore, it is a force controlled treatment that generates compressive residual stresses in the surface layers without modifying the surface topography.

Most investigations have been concentrated on experimentally determining mechanical effects including residual stress field and surface morphology before. Finite Ele-

ment Method（FEM）was initially conducted in the other peening process，such as，Meguid et al. conducted dynamic elasto-plastic analysis of the shot-peening process using a single shot to predict compressive residual stresses in the exposed surface layers in 1999. Hu et al. and Ding and Ye also proposed finite element analyses，instead of a complicated experimental procedure，to predict the development，magnitude and distribution of residual stresses induced by multiple laser shock peening（LSP）.

FEM is first introduced by Kunaporn et al. to investigate the mechanical behavior and predict the residual stresses from water jet peened materials with a commercial FEA software in 2004. A proposed mathematical model based on the multiple impacts of the jets was used to estimate the contact pressure and the feasible peening range. The predicted residual stresses by the FEA model is in a reasonable agreement with the experimental results at the near-surface region.

Attempts were made to investigate the residual stresses induced on materials treated with high-pressure water jet. Rajesh et al. made a transient dynamic finite element analysis，for predicting the residual stresses on material treated with high-velocity water droplets. Impact nature of droplets was simulated by applying impact pressures over a very short duration，estimated using Reichardt's theory and liquid impact theory. Subsequently，a multidroplet impact model，proposed for predicting residual stresses induced on materials subjected to water jet peening，was presented. This approach considers the impact pressure distribution due to high-velocity droplets impinging on the material surface instead of stationary pressure distribution for prediction of residual stresses on water jet-peened surfaces by using transient elastic-plastic finite element analysis. Moreover，Daniewicz and Cummings made a finite element modeling of stationary water jet impinging on an elastic-plastic half-space and performed to characterize WJP processing. Surface residual stresses were found to be a result of subsurface plastic deformations.

Work on the three-dimensional FEM simulation of the process to predict the residual stress field and the surface deformation by WCP is still too little now. A highly-detailed three-dimensional modeling of the entire or partial test specimen would be desirable in order to obtain a more realistic description of residual stress. Considering the reflection and interaction of various impact waves in the different directions of the target materials，a new method to simulate shock wave propagation to predict residual stresses distribution and surface deformation of the material treated by WCP using LS-DYNA and ANSYS in three dimensions is proposed in this paper. FEM modeling strategy is presented in detail. Simulation of several successive impact waves on the same position is performed and discussed. According to the simulation results，residual stress is reckoned after large number of successive shock waves. Effect of different applied impact pressures on the residual stresses is also presented. Finally，the

practical relevance of the proposed approach is shown by comparing the predicted results with the experimental results obtained by WCP.

2 WCP mechanism and experiment procedure

2.1 WCP mechanism

Water is supplied by a pump to the water jet from the reservoir tank. The pressure and the flux of the plunger pump are 30 MPa and 16 L/min, respectively. The nozzle with the inner diameter of 1 mm can be pressed by a small air pump, and its flux is adjustable from 0 L/min to 1.0 L/min. Test specimen is positioned near the bottom of test water tank, and the jet direction is normal to the surface of test specimen. During the process of WCP, the test tank is filled with water. The temperature of the working water is kept at 293-297 K. When the high-pressure water is jetted in the vertical direction from a jet nozzle to the top of tank, the uniform big bubble cloud can be generated and the bubble collapse on the surface of the specimen will produce impact effect just as shotpeening.

2.2 Experiment procedure

A pure titanium specimen was treated with duration of 15 min by WCP. As shown in Fig. 1, the size of test specimen was 80×80×10 mm^3. An enhancement zone of ϕ24 mm was obtained. The depth distribution of residual stress in the near-surface layer was measured by X-ray diffraction stress analysis using the conventional $\sin^2\Psi$ method. A side inclination method was also used for stress measurement. The X-ray tube (Co Kα type) was operated at 30 kV and 10 mA, with a slit diameter of 2 mm. The shift of theα-Ti (114) diffraction profile was detected at anglesφ=10°, 20°, 30°, 40° and 45°. The diffractive angle $2\theta_0$ was 154.4°. The stress constant of the X-ray diffraction analysis was −180 MPa/°. The near-surface layer of the test point was removed by step-by-step electrolytical polishing using a Proto Electrolytic Polisher-Model 8818 (Proto Manufacturing Ltd.). Experiment results are used as a reference to validate the FEM results of the simulation.

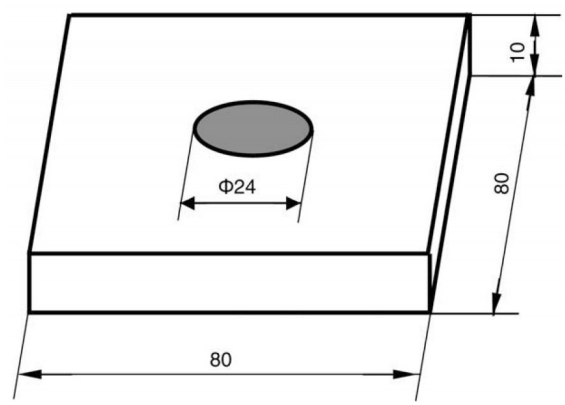


Fig.1 The geonmetry and dimensions of the specimen

3 FEM simulation strategy

3.1 Material

Residual stresses in materials are often the result of macroplastic deformation and

micro-plastic deformation accompanying the microstructure changes. Recently, author investigated the water cavitation peening-induced microstructures and distributions of residual stress in the near-surface layer of pure titanium. The results indicated the distributions of residual stress were good agreement with the density of twinning and dislocations near-surface layer of pure titanium. In order to keep the continuity of the research, the pure titanium was selected as an example for evaluation. The pure titanium was selected as an example for evaluation. The specimen was a rectangle solid with size of 80×80×10 mm^3, and it is also considered as an isotropic and perfect elastic-plastic material. The mechanical properties are summarized in Table 1.

3.2 Analytical model

Under uniaxial strain conditions, the highest elastic stress level in the impact wave propagation is defined as the Hugoniot Elastic Limit (HEL). When the applied stress is greater than HEL, permanent deformation occurs. Assuming that the yielding occurs when the applied stress in the direction of the wave propagation exceeds the HEL, the dynamic yield strength σ_y^{dyna} under uniaxial strain conditions can be defined in terms of the HEL by:

$$\sigma_y^{dyna} = HEL\frac{(1-2v)}{(1-v)} \tag{1}$$

Where ν is Poisson's ratio. Also, the target material is assumed to be perfect elastic-plastic with isotropic and homogeneous characteristics for analysis. The plastic strain is assumed to follow the Von Mises yielding criterion and the dynamic yield strength σ_y^{dyna} is based on Eq. (1).

According to Hook's law, the surface plastic strain ε_{plas} can be expressed as:

$$\varepsilon_{plas} = \frac{-2HEL}{3\lambda+2\mu}\left(\frac{P}{HEL}-1\right) \tag{2}$$

Where P is the impact pressure, λ and μ are Lame's constants. The residual stress induced by WCP can be written as:

Table 1 Mechanical properties of pure titanium.

Properties	Value	Unit
Density (ρ)	4.51×10^3	kg/m^3
Poisson's ratio (ν)	0.34	—
Elastic modulus (E)	1.08×10^5	MPa
Hugoniot elastic limit (HEL)	1.15×10^3	MPa

$$\sigma_{resi} = \sigma_0 - \left[\frac{\mu\varepsilon_p(1+v)}{(1-v)} + \sigma_0\right]\left[1-\frac{4L_p(1+v)}{\pi r_p}\right] \tag{3}$$

where r_p is radius of impact zone, σ_0 is initial residual stress, L_p is the depth of

需要全本请访问 www.ertongbook.com

plastic affection. It can be defined as:

$$L_p = \left(\frac{C_l^e C_l^p \tau}{C_l^e - C_l^p} \right) \left(\frac{P - HEL}{2HEL} \right) \tag{4}$$

Where τ is pressure pulse duration, C_l^e and C_l^p are elastic and plastic velocities, respectively. C_l^e and C_l^p can be defined as:

$$C_l^e = \sqrt{\frac{(1-v)\ E}{(1+v)\ \ (1-2v)} \cdot \frac{1}{\rho}} \tag{5}$$

$$C_l^p = \sqrt{\frac{E}{3(1-2v)}} \cdot \frac{1}{\rho} \tag{6}$$

Where ρ is material density.

3.3 Finite element model

The three-dimension semi-infinite finite element model with size $40 \times 40 \times 40$ mm^3 was created to simulate the residual stress induced by WCP. Since the model is symmetric and subjected to a symmetric uniform circular pressure pulse, only a quarter of the configuration is used to perform the finite element calculation instead of the whole to improve computational efficiency.

A schematic configuration of this model including boundary conditions is shown in Fig. 2. The symmetric boundary conditions are employed on the *x*-0-*z* and 0-*y*-*z* planes. Nonreflecting boundaries, which will prevent stress wave reflections generated at the boundary from re-entering the model and contaminating the results, are applied to the exterior surfaces of the model to simulate the semi-infinite model.

The Solid 164 element with an 8-node brick element is chosen. By default, it uses reduced (one point) integration plus viscous hourglass control for faster element formulation. One point integration is advantageous due to savings on computer time and robustness in cases of large deformations. Results of FEM analysis are sensitive to the mesh density. It is easy to obtain more accurate results with dense meshes, but higher computational cost. To accurately capture mechanical effects induced by impact waves, it is necessary to have sufficient mesh density about the region subjected to impact waves. As shown in Fig. 2, a densely meshed region is plot near the impact zone with the element edge length of 0.75 mm in *x*-direction

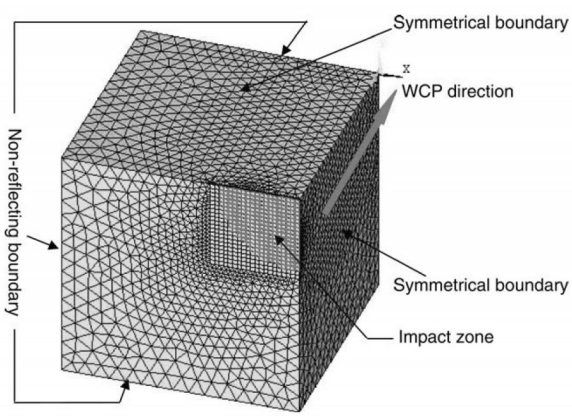


Fig.2 Schematic of bundary condition on finite element model.

and *y*-direction, and 0.025 mm in *z*-direction. The number of elements in the densely meshed region is 8000. For the rest region, mesh density is about three times as coarse as the densely meshed one. The number of total elements in model is 62,526.

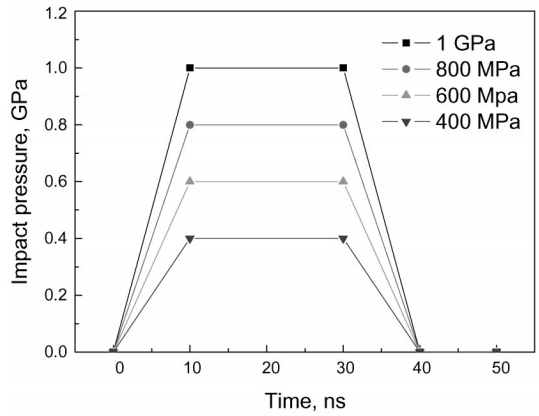


Fig.3 Impact wave load changes as a function of time.

The high amplitude, short duration pressure pulse of impact wave generated by WCP is one of key parameters related to the residual stress induced by WCP. The pressure sources is impact waves due to cavitation collapse. The highest amplitude of impact wave is about up to 1.2-1.4 MPa, which was measured by the pit number on surface of metal materials induced by cavitation. The amplitude of impact wave is above 320 MPa, which was measured by a pressure sensitive film in WCP process. The impact pressure of 400 MPa, 600 MPa, 800 MPa, and 1 GPa were investigated in this study. The load curve of trapeziform wave is shown in Fig. 3. The duration of impact wave is 40 ns, and the solution time is 1×10^4 ns. Simulation of 50 times successive impact waves on the same position is performed.

4 Results and discussion

4.1 Simulation results and discussion

In general, plastic deformation is a result of the "non-recovery" of material after unloading. For the elastic-plastic material, if the load is applied within the elastic range of the curve, the material will completely recover after unloading. However, if the applied load is beyond the elastic range, the material starts yielding and after unloading, plastic deformation is exhibited through unrecovered or plastic strain, which result in residual stresses in the material. *X*-stress σ_x, *Y*-stress σ_y, denotes the stress component in *X*-direction and *Y*-direction, respectively. According to the Von Mises criterion, the effective stress σ_e can be computed from the different stress components. The effective stress σ_e also is referred to as Von Mises stress in this study. Contours of the Von Mises stress distribution of the single impact wave dynamic analysis at 1×10^3 ns, 1.5×10^3 ns, and 1×10^4 ns are shown in Fig. 4. From Fig. 4a and c, with the increase of solution time, the maximum of Von Mises stress has decreased from 228.3 MPa to 207.2 MPa due to the recovery of the elastic strain. After the sufficient interaction of stress waves, the static residual stress field formed in subsurface of material as observed in Fig. 4c.

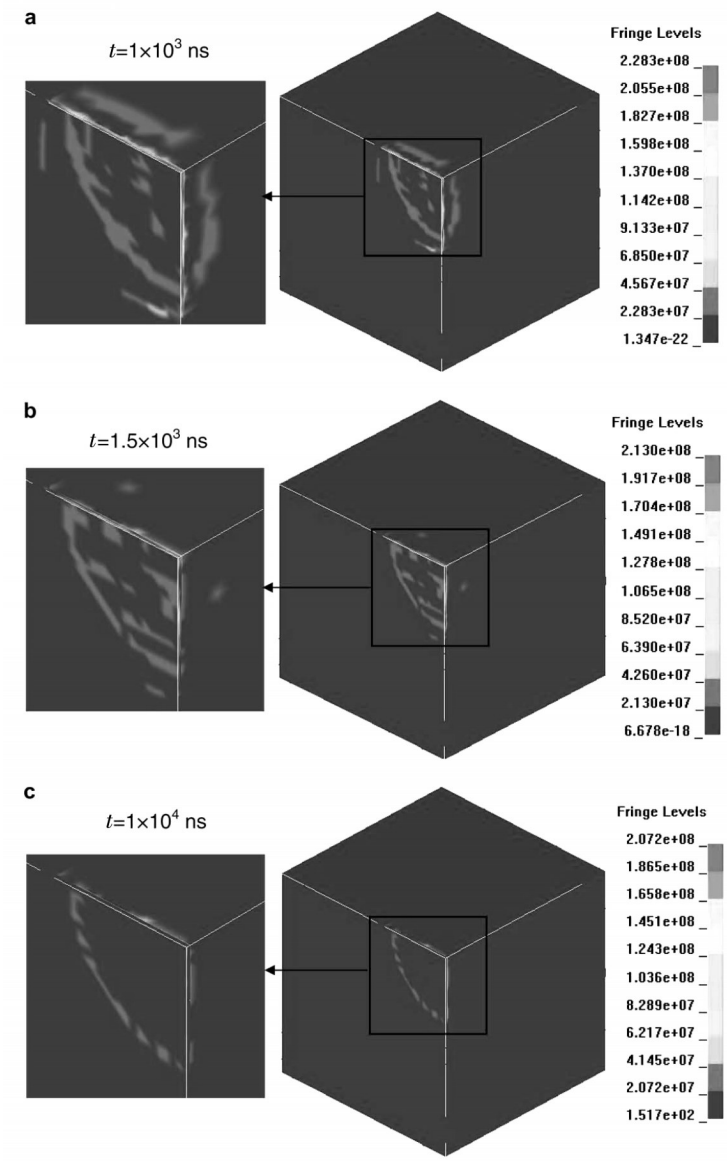


Fig.4 Contour of Von Miss distribution of single impact wave

In WCP process, the successive interval impact waves are assumed to apply to the peened surface of material. *X*-stress σ_x dynamic evolution at different element (element No. 3193 and No. 3153) resulting from the five impact waves is shown in Fig. 5. Element No. 3193 is the surface element in the impact zone, and element no. 3153 is along the impact direction in depth of 50 μm. According to Fig. 5, residual stress repeatedly shakes between compressive stress and tension stress. From the beginning to the end of single impact wave duration, the amplitude of stress is decaying before $5e\times10^3$ ns, and is driven to be stable after 5×10^3 ns. The stable residual stresses form at 1×10^4 ns resulting from the plastic strain. The values of residual stress in-

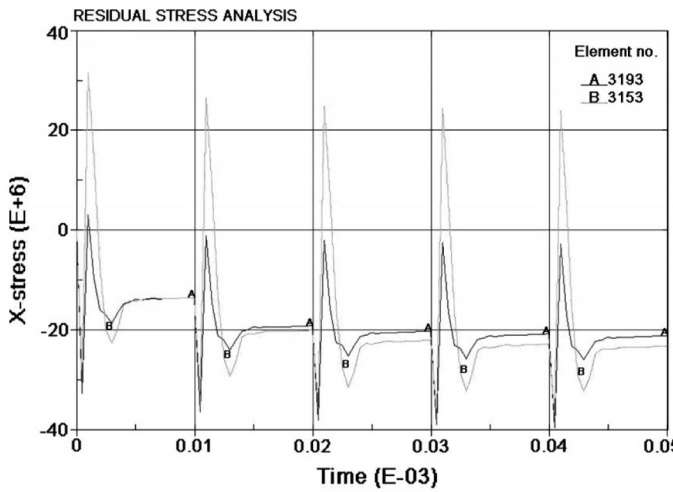


Fig.5 Residual X-stress dynamic change as a function of time at different element (the first 5 impact waves)

crease gradually with increasing the number of impact wave. The residual stress fields after fifty impact waves are shown in Fig. 6. Compressive residual stresses increase by the multiple impact waves. The maximum of the Von Mises stress increase by 24.5% from 207.2 MPa to 257.9 MPa.

Residual *Y*-stresses σ_y of different node as a function of impact wave number with different applied pressure are shown in Fig. 7. In impact affected zone, the surface node No. 1141 is adopted primarily. Subsequently the next is at interval of 25 μm along the impact direction, the node number is 1141, 7083, 7064, 7045, 7026, 7007 and 6988, respectively. Distribution rules of residual stresses with different applied pressure are basically same. Magnitude of residual stress is relatively driven to be stable with the tiny increment after 10 impact waves, which indicate the predicting of residual stress is feasible. A detail discussion will be given in Section 4.2.

Residual *Y*-stresses σ_y as a function of depth with different applied pressure and impact number are shown in Fig. 8. From Fig. 8, it can be observed that the maxima of the compressive residual stresses are at the subsurface 50 μm. While the maxima of the residual stress increment on surface are a little larger than that of the subsurface. Residual stress distribution is stable after 10 impact waves. The surface compressive residual stresses under peak of impact pressure increase from −11.88 MPa to −22.20 MPa, from −9.63 MPa to −18.02 MPa, from −7.32 MPa to −13.71 MPa, and from −4.95 MPa to −9.18 MPa after 50 impact waves, respectively. The plastically affected depth is about up to 120 μm. The depth of compressive residual stress is around up to 80 μm.

4.2 Predicting residual stress and validation

In order to predict residual stress after 15 min WCP time, the number of impact waves $N_{\min}$ induced by WCP in 1 min is assumed. Parameter $N_{\min}$ can be defined as:

$$N_{\min}=\frac{(N_{air}+N_{water})C_2}{N_{wave}}=\frac{\left(Q_{water}C_1/V_{bubb}+Q_{air}/V_{bubb}\right)C_2}{\pi D^2/\pi d^2} \tag{7}$$

Where, N_{air} is the bubble number induced by air, N_{water} is the bubble number induced by water, N_{wave} is the bubble number which can generate one impact wave, Q_{water} is the flux of plunger pump, Q_{air} is the flux of air pump, V_{bubb} is the volume of bubble, C_1 is the ratio of generating nucleus, C_2 is the ratio of effective bubble, D and d is the diameter of impact zone and bubble, respectively. In this study, the values of the above parameters are listed in Table 2. According to Eq. (7), $N_{\min}$ can be calculated, the values range from 220-450.

After WCP duration of n min, residual stress R^n_{pred} is predicted by:

$$R^n_{pred}=nN_{\min}R^5_{incre} \tag{8}$$

Where, R^5_{incre} is the average increment of the last 5 impact wave in simulation results. The limitation of such an approach is that WCP duration is less than the saturation duration. Saturation duration depends on the characteristics of materials and WCP process parameters. The precision is irresponsible when WCP duration of Nmin is more than the saturation duration of materials.

According to the above formula, the residual stresses after WCP duration of 15 min are predicted. The predicting results and experimental results are shown in Fig. 9. For assessing the practical relevance of the proposed model, the results predicted with the model are compared with experimental results obtained by WCP. It can be seen that the distribution tendency of predicted results is almost same under different applied impact pressure. Comparison to the experiment results, the predicted results with the applied impact pressure of 400-600 MPa have good agreements. Only the measurement residual stress in the depth of 0-50 μm is higher than that of the predicted results. Generally, two types of residual stresses should be considered, that is, macro-residual stresses and micro-residual stresses. In the proposed model, micro-residual stresses components induced by micro-plastic deformation such as high density dislocations is not consider, which cause the different distribution shape of residual stress between the predicting results and the experimental results. Micro-plastic deformations such as high density dislocations usually cause the compressive residual stresses. Considered micro-residual stresses components induced by the high density dislocation in the depth of 0-50 μm, the predicted results with applied impact pressure around 400-600 MPa are in a reasonable agreement with the experimental results.

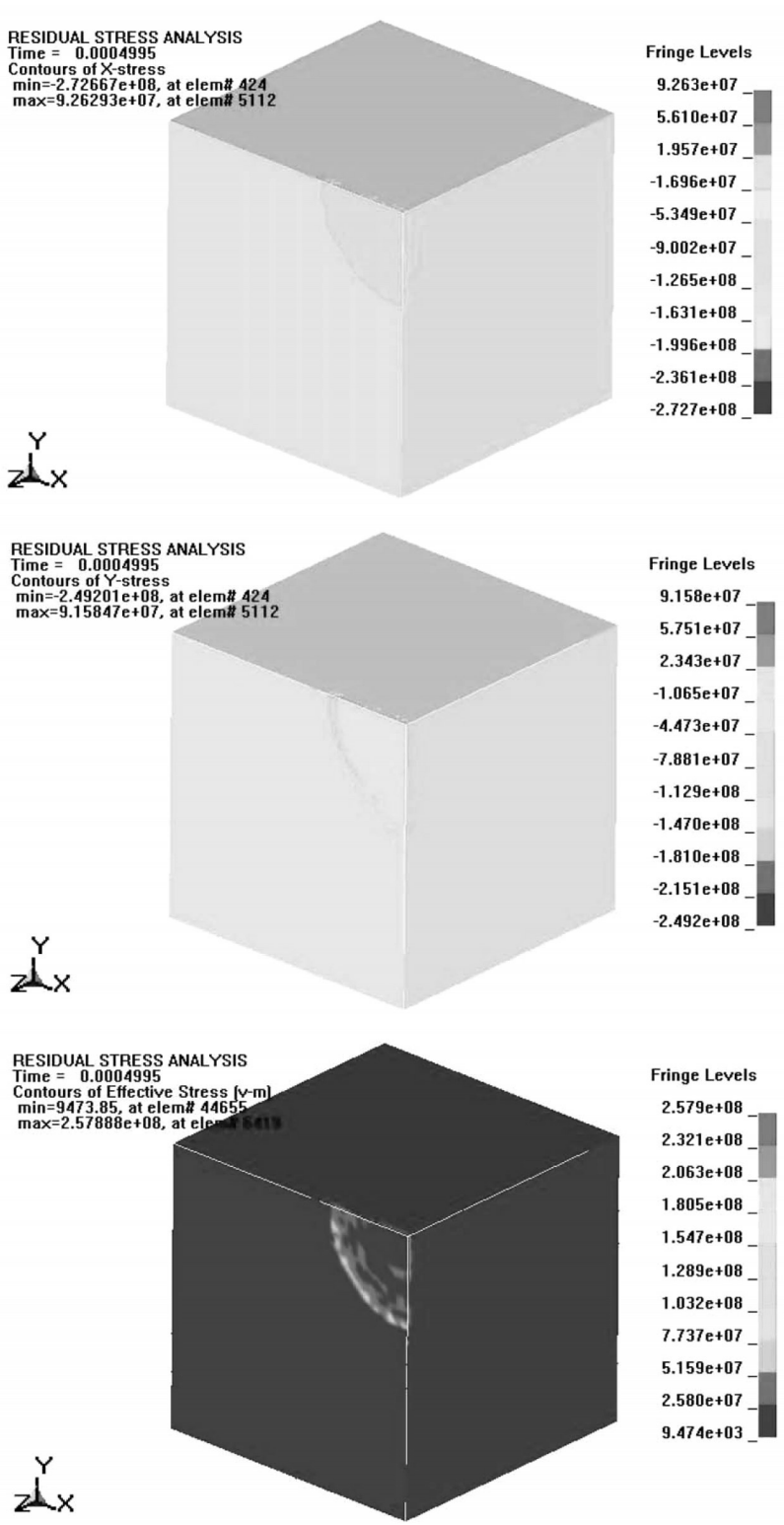


Fig.6 Residual stress field after the 50th impact wave

需要全本请访问 www.ertongbook.com